JOURNAL OF GEOPHYSICAL RESEARCH, VOL. 111, B06410, doi:10.1029/2005JB004094, 2006

Accretionary prisms in subduction earthquake cycles: The theory of dynamic Coulomb wedge

Kelin Wang[1,2] and Yan Hu[2]

Received 7 October 2005; revised 3 March 2006; accepted 17 March 2006; published 27 June 2006.

[1] We expand the theory of critically tapered Coulomb wedge for accretionary prisms by considering stress changes in subduction earthquake cycles. Building on the Coulomb plasticity of the classical theory, we assume an elastic–perfectly Coulomb plastic rheology and derive exact stress solutions for stable and critical wedges. The new theory postulates that the actively deforming, most seaward part of an accretionary prism (the outer wedge) overlies the updip velocity-strengthening part of the subduction fault, and the less deformed inner wedge overlies the velocity-weakening part (the seismogenic zone). During great earthquakes, the outer wedge is pushed into a compressively critical state, with an increase in basal and internal stresses and pore fluid pressure. After the earthquake, the outer wedge returns to a stable state. The outer wedge geometry is controlled by the peak stress of the updip velocity-strengthening part of the subduction fault achieved in largest earthquakes. The inner wedge generally stays in the stable regime throughout earthquake cycles, acting as an apparent backstop and providing a stable environment for the formation of forearc basins. The new theory has important implications for the studies of the updip limit of the seismogenic zone, the evolution of accretionary prisms and forearc basins, activation of splay faults and tsunami generation, evolution of the fluid regime, and mechanics of frontal prisms at margins dominated by tectonic erosion.

Citation: Wang, K., and Y. Hu (2006), Accretionary prisms in subduction earthquake cycles: The theory of dynamic Coulomb wedge, *J. Geophys. Res.*, *111*, B06410, doi:10.1029/2005JB004094.

1. Introduction

[2] The theory of critically tapered Coulomb wedge [*Davis et al.*, 1983; *Dahlen*, 1990] has met great success in its application to deformation processes at convergent margins. Some of the applications to submarine wedges are summarized in Table 1. However, not addressed by the theory is one of the most important processes in subduction zones: great earthquakes. It is the purpose of the present work to expand the classical Coulomb wedge theory and to establish a conceptual framework for studying mechanical processes of submarine wedges throughout earthquake cycles.

[3] As applied, the classical Coulomb wedge theory describes an end-member scenario in which the subduction fault slips at a constant shear stress and the wedge is in a critical state. Except for the rare situation of purely aseismic subduction, the theory is understood to address a long-term process averaged over numerous earthquake cycles. In this work, we begin by considering the other end-member scenario in which the subduction fault alternates between interseismic locking and coseismic slip. End-member scenarios simplify the physics and help us understand the real situation that may involve slip of various parts of the subduction fault at variable rates and different timescales. We also use a two-dimensional simplification (Figure 1b) of the three-dimensional system in which the fault may show downdip and along-strike variations in its seismogenic behavior at various scales (Figure 1a) [*Bilek and Lay*, 2002].

[4] The seismogenic portion of a subduction fault exhibits a velocity-weakening behavior, that is, its frictional resistance against slip decreases with increasing slip rate. The shear stress on the fault builds up toward the level of failure when the fault is locked, but the stress may drop to a very small value during an earthquake (Figure 1c). Because seismic rupture of subduction faults does not extend all the way to the trench (or deformation front of accretionary prisms), the most updip segment of the faults must have a velocity-strengthening behavior. During most part of an interseismic period when the seismogenic zone is locked, this updip segment may have little or no slip rate [*Wang and Dixon*, 2004], and hence the shear stress on the fault may become low. During an earthquake when the updip segment is forced to slip by the rupture of the downdip seismogenic zone, its strength must increase to resist slip (Figure 1c) [*Marone and Saffer*, 2006].

[5] Fluctuations of fault stress in earthquake cycles must affect wedge mechanics. Because of the fluctuation of basal stress, the wedge cannot always be in a critical state, and

[1]Pacific Geoscience Centre, Geological Survey of Canada, Sidney, British Columbia, Canada.
[2]School of Earth and Ocean Sciences, University of Victoria, Victoria, British Columbia, Canada.

0148-0227/06/2005JB004094$09.00

Table 1. Some Applications of Classical Coulomb Wedge Theory to Submarine Wedges

Reference	Subduction Zones	μ	μ_b	Notes
Davis et al. [1983]	Japan, Java, Sunda, Peru, Makran, Aleutian, Barbados, Oregon	1.03	0.85	$\lambda = \lambda_b$
Dahlen [1984]	above Guatemala	1.1	0.85	$\lambda = \lambda_b$
Zhao et al. [1986]	Mostly Barbados	0.85, 0.4	0.85, 0.4	$\lambda = \lambda_b$, $\mu = \mu_b$
Davis and von Huene [1987]	Aleutian	0.45	0.3–0.45	$\lambda \leq \lambda_b$
Dahlen [1990]	Barbados	0.27–1.57	0.27–0.85	$\lambda = \lambda_b = 0.95$
Breen and Orange [1992]	Barbados	0.45–1.1	0.45,0.85	
Lallemand et al. [1994]	21 trenches	0.52	$\mu_b'' = 0.029$	$\lambda = 0.88$
Adam and Reuther [2000]	northern Chile	0.7	0.7	λ, $\lambda_b \leq 0.83$
Kukowski et al. [2001]	Makran	0.42	0.22	$\lambda = 0.42$–0.6
Saffer and Bekins [2002]	Mexico, Cascadia, Nankai, Nankai	0.85	0.55, 0.85	$\lambda = \lambda_b$ (variable)
Hayward et al. [2003]	Barbados	0.85	0.85	$\lambda \approx$ hydrostatic
Kopp and Kukowski [2003]	Sunda	0.31	0.135	$\lambda \approx \lambda_b = 0.47$

therefore the mechanics of a stable wedge also needs to be considered. In this work, we assume an elastic–perfectly Coulomb plastic rheology, derive stress solutions for both critical and stable regimes, and propose a theory of dynamic Coulomb wedge. Although the theory is based on static stress equilibrium and ignores inertial forces and seismic wave propagation, we use the word "dynamic" to emphasize the importance of temporal changes in the state of stress and deformation mechanism (elastic versus plastic).

[6] This paper focuses on accretionary prisms, but with some modification the theory can be applied to wedges composed of crystalline rocks, as is observed at margins dominated by subduction erosion [*von Huene and Scholl*, 1991].

2. Observed Wedge Geometry and Deformation Style of Accretionary Margins

[7] Critical to understanding the mechanics of accretionary wedges is the observation of a sharp contrast in structural style between their seaward (a few tens of kilometers) and landward parts. Cross sections of two margins are shown in Figure 2 as examples. There are significant variations in wedge geometry along each margin [e.g., *Gulick et al.*, 2004], but the sections shown in Figure 2 are considered representative. Similar geometry and structure have been reported for Cascadia [*McNeill et al.*, 1997; *Gulick et al.*, 1998], Hikurangi [*Beanland et al.*, 1998], Makran [*Kukowski et al.*, 2001], Sunda [*Kopp and Kukowski*, 2003], and many other margins [*Clift and Vannucchi*, 2004].

[8] The near-trench part, referred to as the outer wedge, is often characterized by a series of imbricate thrust faults, a subject of many observational, experimental, and theoretical studies [e.g., *Mandal et al.*, 1997; *Lohrmann et al.*, 2003; *Gulick et al.*, 2004]. The inner wedge further landward, which consists of older accreted sediments and margin rock framework and has no clearly defined landward boundary, often hosts forearc basins overlying materials of a former outer wedge. The near absence of contractile structure in these forearc basins and hence the lack of active permanent shortening of the inner wedge is a striking feature of the forearc system that has prompted several investigations [e.g., *Byrne et al.*, 1988; *von Huene and Klaeschen*, 1999]. Rupture zones of great earthquakes tend to underlie the inner wedge [*Wells et al.*, 2003]. The outer wedge usually has a steeper surface slope than does the inner wedge (disregarding the very low slope of the "proto-wedge" sometimes observed near the trench). The slope break can be rather distinct at some margins (Figure 2a). For margins dominated by subduction erosion, the most seaward part of the outer wedge usually is a small sediment prism, called the frontal prism, while the rest of the outer wedge is part of the margin rock framework. The frontal prism is similar to outer accretionary wedges shown in Figure 2 and will be discussed in section 5.5.

[9] The Nankai section in Figure 2a [*Park et al.*, 2002] is in the region of the 1944 M_w 8.1 Tonankai earthquake rupture area [*Ando*, 1975]. The inner wedge has a flat upper surface. The Alaska section (Figure 2b) [*von Huene and Klaeschen*, 1999] lies between the two high-slip areas of the rupture zone of the 1964 M_w 9.2 great Alaska earthquake [*Christensen and Beck*, 1994]. The slope break is not as distinct as for the Nankai profile or for profiles to the northeast along the Alaska margin [*Fruehn et al.*, 1999], but the contrast in deformation style across it is as sharp. Through geometrical restoration of thrust sections, *von Huene and Klaeschen* [1999] showed that over the past 3 Myr, nearly all the permanent compressive deformation took place within 30 km of the trench, with little deformation beyond 40 km.

[10] What is responsible for the transition from the severely compressive outer wedge to the less compressive inner wedge and the often distinct slope break? The classical critical wedge theory, assuming steady slip of the plate interface against constant resistance, predicts that a greater surface slope is indicative of a stronger basal fault or a weaker wedge material.

[11] For a steadily slipping subduction fault, the segment beneath the outer wedge is expected to be no stronger than further downdip. *Byrne et al.* [1988] thus reasoned that the outer-inner wedge structural contrast must be due to a contrast in the strength of the wedge material. They introduced a strong crystalline basement backstop gently sloping seaward and extending to the slope break, enhancing the apparent strength of the inner wedge. The strong basement serves as a "backbone" to protect the overlying formations from permanent shortening. This model applies very well to margins that have small sedimentary prisms such as those dominated by subduction erosion. However, the crystalline backstop is usually absent, or farther landward than the area of structural transition and slope break, at accretion-

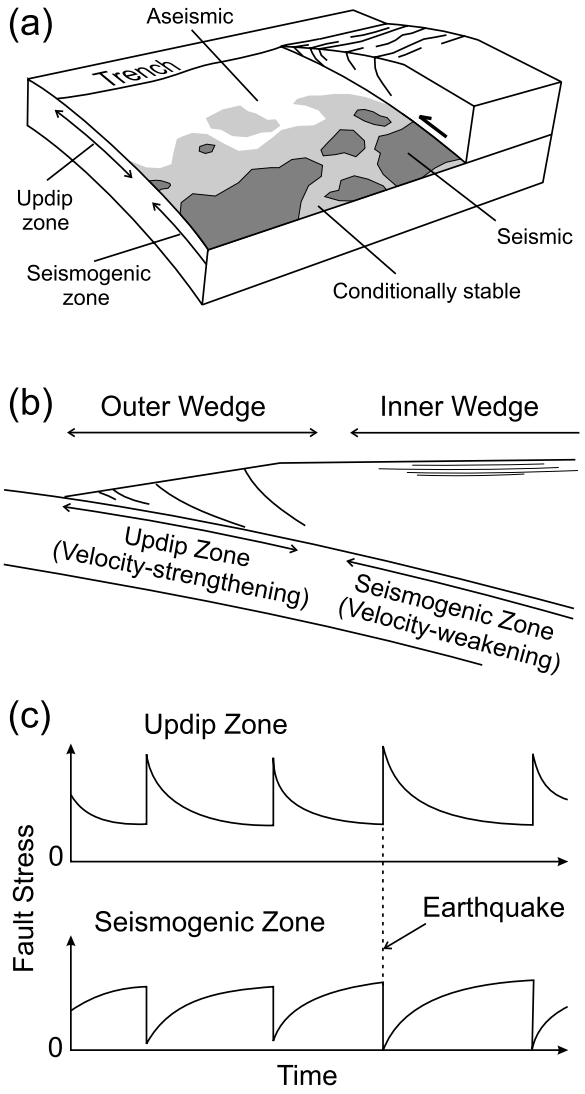

Figure 1. (a) Cartoon showing spatial variations in seismogenic behavior of a subduction fault, based on a similar figure by *Bilek and Lay* [2002]. (b) Two-dimensional simplification of the system shown in Figure 1a. (c) Schematic illustration of shear stress variations along the two parts of the fault shown in Figure 1b. Coseismic stress drop in the seismogenic zone is accompanied with stress increase in the updip segment.

dominated margins like Nankai and Alaska (Figures 2a and 2b). Therefore a different explanation is needed.

[12] It also has been proposed that a backstop could consist of more consolidated, and hence stronger, sediment instead of crystalline basement rocks. *Kopp and Kukowski* [2003] named this type of backstop the "dynamic" backstop to distinguish it from the basement backstop. However, as indicated by reported seismic velocities for the profiles in Figure 2, landward increase in the consolidation state appears to be more gradual than reflected in the structural contrast or a slope break.

[13] In section 4, we will show that the wedge geometry and deformation style discussed above can be readily explained using the dynamic Coulomb wedge theory. Because the new theory is built on the classical theory, we first summarize the classical theory and its application to accretionary prisms in section 3.

3. Classical Coulomb Wedge Theory

3.1. Stress Solution

[14] Here we summarize the widely used exact stress solutions of *Dahlen* [1984] and *Zhao et al.* [1986], although various simpler or more refined analytical and numerical versions are also available [*Davis et al.*, 1983; *Dahlen et al.*, 1984; *Fletcher*, 1989; *Dahlen*, 1990; *Breen and Orange*, 1992; *Willett et al.*, 1993; *Wang and Davis*, 1996; *Enlow and Koons*, 1998]. Exactly the same formulation will be used for our new stress solution in section 4.

[15] Consider a two-dimensional wedge with an upper slope angle α and basal dip β in the (x, y) coordinate system illustrated in Figure 3. The wedge is subject to gravitational force ρg, where ρ is the density of the wedge material and g is gravitational acceleration. Pore fluid pressure P within the wedge is parameterized using a generalized Hubbert-Rubey fluid pressure ratio defined as [*Dahlen*, 1984]

$$\lambda = \frac{P - \rho_w g D}{-\sigma_y - \rho_w g D} \tag{1}$$

where D and ρ_w are water depth and density ($\rho_w = 0$ for a subareal wedge), respectively, and σ_y is normal stress in the y direction (negative if compressive). It is assumed that shear stress τ_n and normal stress σ_n on the basal fault obey the friction law [*Dahlen*, 1984]

$$\tau_n = -\mu_b(\sigma_n + P_b) = -\mu_b'(\sigma_n + P) = -\mu_b'\overline{\sigma}_n \tag{2}$$

where $\overline{\sigma}_n = \sigma_n + P$ is the effective normal stress just above the basal fault, P_b is pore fluid pressure along the basal fault, $\mu_b = \tan \varphi_b$ is the coefficient of basal friction, and $\mu_b' = \tan \varphi'_b$ is the effective coefficient of basal friction defined as

$$\mu_b' = \tan \varphi_b' = \frac{\mu_b''}{1 - \lambda} \tag{3}$$

where μ_b'' is a basal friction property that depends on both the intrinsic basal friction coefficient μ_b and the effect of pore fluid pressure within the fault zone. If a basal fluid pressure ratio λ_b similar to λ in physical meaning is properly defined, we can have $\mu_b'' = \mu_b(1 - \lambda_b)$. A negative μ_b'' represents a normal fault [*Xiao et al.*, 1991].

[16] If the wedge is uniformly Coulomb plastic with its cohesion proportional to depth and is everywhere on the verge of failure, an exact stress solution can be obtained [*Zhao et al.*, 1986]. If we write cohesion S_0 in the following form:

$$S_0 = \eta(1 - \lambda)\mu\rho g y \cos\alpha \tag{4}$$

where the cohesion gradient η is a dimensionless constant and $\mu = \tan \varphi$ is the coefficient of internal friction, the

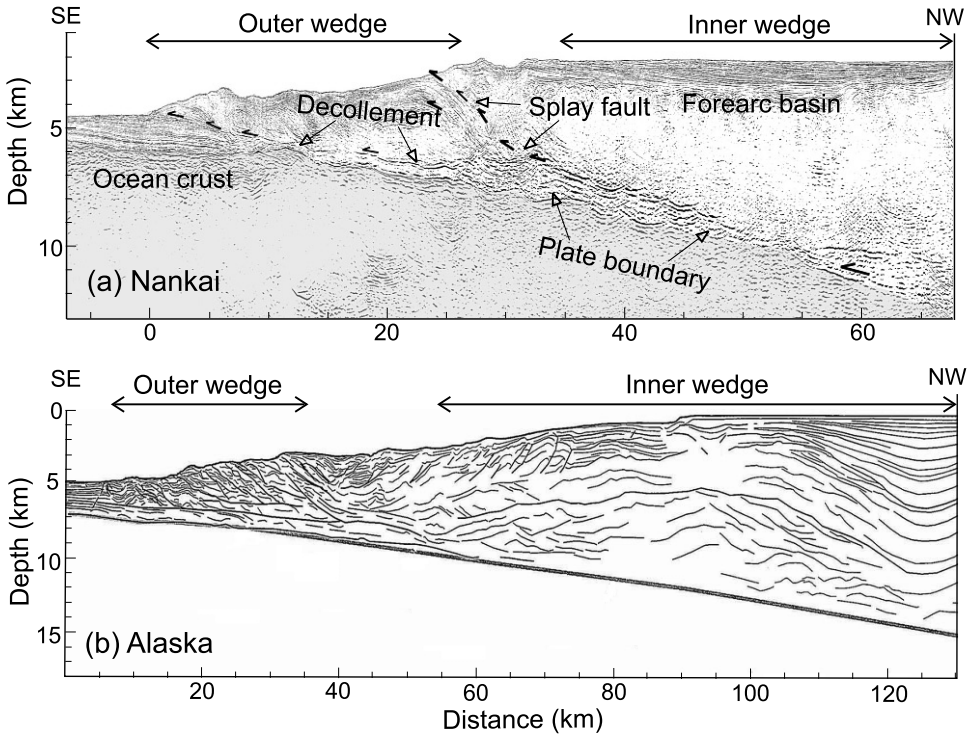

Figure 2. Published structure and geometry of two accretionary wedges. The degree of detail depends on information provided in the original publications. The outer-inner wedge transition is narrow relative to the size of the outer wedge, but the transition cannot be defined by a vertical line. (a) Nankai, based on a seismic profile off the Kii Peninsula [*Park et al.*, 2002]. (b) Alaska, based on a seismic profile between the Kenai Peninsula and Kodiak Island reported by *von Huene and Klaeschen* [1999], who determined that permanent shortening over the past 3 Myr occurred nearly all within the most seaward 30–40 km (outer wedge).

solution of *Zhao et al.* [1986], in terms of effective stresses, can be written as

$$\overline{\sigma}_x = -m^c(1-\lambda)\rho g y\cos\alpha \tag{5a}$$

$$\overline{\sigma}_y = -(1-\lambda)\rho g y\cos\alpha \tag{5b}$$

$$\tau_{xy} = (1-\rho')\rho g y\sin\alpha \tag{5c}$$

where $\rho' = \rho_w/\rho$ and

$$m^c = 1 + \frac{2(1+\eta)}{\csc\varphi\sec 2\psi_0^c - 1} \tag{6}$$

with ψ_0^c being the uniform angle between the most compressive principal stress σ_1 and the upper surface. ψ_0^c is given by the following relation

$$\frac{\tan 2\psi_0^c}{\csc\varphi\sec 2\psi_0^c - 1} = \frac{\tan\alpha'}{1+\eta} \tag{7}$$

where

$$\tan\alpha' = \frac{1-\rho'}{1-\lambda}\tan\alpha \tag{8}$$

is the constant ratio of $\tau_{xy}/(-\overline{\sigma}_y)$ ("modified surface slope" of *Dahlen* [1984]). Note that $\overline{\sigma}_x = m^c\overline{\sigma}_y$, $\tau_{xy} = -\overline{\sigma}_y \tan\alpha'$, and $S_0 = -\eta\mu\overline{\sigma}_y$. The taper angle of the critical wedge is

$$\alpha + \beta = \psi_b^c - \psi_0^c \tag{9}$$

where ψ_b^c is the angle between σ_1 and the basal surface and is directly related to μ_b' as well as μ. For $\eta = 0$, the

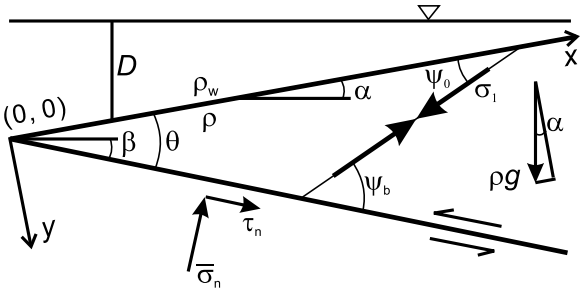

Figure 3. Schematic illustration of a critical or stable wedge to show the coordinate system (x, y), maximum compressive stress σ_1, angles α, β, ψ_0, and ψ_b, water depth D, and basal tractions. In a critical state, ψ_0 and ψ_b become ψ_0^c and ψ_b^c, respectively.

above solution reduces to that of a noncohesive Coulomb wedge earlier obtained by *Dahlen* [1984].

3.2. Application of the Classical Theory to Accretionary Wedges

[17] Classical Coulomb wedge models of accretionary prisms describe a time-averaged state. Just how stress variations are averaged through earthquake cycles over time is not defined, so the use of presently observed values for some parameters such as λ, μ_b, and μ_b'' requires appropriate qualification. The models provide a "reference state" for later discussions, but changes in wedge and fault parameters in subduction earthquake cycles are more important than their reference values, as we will discuss in section 4.

[18] A wide range of μ values has been assumed (Table 1). High values such as 0.85 and 1.1 are appropriate for crystalline or well-consolidated sedimentary rocks. Low values such as 0.31, 0.42, and 0.45 have been determined from angles of pristine conjugate faults near the wedge toe and therefore are appropriate for soft sediments being accreted. An average value for the entire wedge may be somewhere in between, such as 0.6–0.7. The two sets of conjugate seafloor-cutting normal faults just landward of the slope break (not discernable in Figure 2a but clearly shown in an inset of *Park et al.* [2002]) are obviously pristine and represent in situ internal friction. The angle between the two sets is 55° (J. Park, personal communication, 2005), which gives μ = 0.7. The average degree of consolidation in frontal prisms at margins dominated by subduction erosion may be lower, and smaller μ values may be more appropriate for them.

[19] There is evidence that μ_b of materials in a slowly slipping subduction fault zone is substantially lower than μ of the overlying wedge [*Henry*, 2000; *Brown et al.*, 2003; *Moore and Lockner*, 2006]. Muddy faults may have very low fault-normal permeability, making it easier for them to stay overpressured [*Dewhurst et al.*, 1996]. The elevated pore fluid pressure further weakens the fault zone.

[20] By considering forearc stress orientation and force balance, *Wang and He* [1999] determined the present (interseismic) μ_b'' value to be around 0.03–0.05 for the Nankai and Cascadia subduction zones. On a shallowly dipping subduction fault, a value of μ_b'' = 0.04 gives a shear stress of around 20 MPa at 20 km depth. The low shear stress is consistent with the state of stress near the Japan Trench [*Magee and Zoback*, 1993] and low frictional heating on the Cascadia subduction fault [*Wang et al.*, 1995].

[21] On the basis of above discussions, we use μ = 0.7 and μ_b'' = 0.04 for the reference wedge model. For outer wedges, it is reasonable to assume η = 0 (noncohesive). In the $\alpha - \beta$ plot in Figure 4, we show the trajectory of pairs of critical α and β values for λ = 0.5 (solid lines). The lower branch of the trajectory represents compressively critical states, and the upper one represents extensionally critical (gravitational collapse) states. They encompass a stable region. Critical states for a rather weak wedge (λ = 0.88, μ = 0.52, and μ_b'' = 0.029) as used in *Lallemand et al.* [1994] are also shown for comparison.

[22] The outer wedges of the two margins in Figure 2 and sedimentary wedges discussed by *von Huene and Ranero* [2003] are shown in the same plot. The northern Chile frontal prism, also shown in this plot, will be discussed in section 5.5. Slope angle and basal dip values used in some previous reviews may not be representative of outer wedges or frontal prisms and are not shown here. For example, *Lallemand et al.* [1994] took the average between the trench and where the plate interface is 10 km deep, and *Clift and Vannucchi* [2004] used a wedge geometry averaged over a distance of at least 50 km measured from the trench. These approaches usually resulted in an underestimate of the surface slope and overestimate of the basal dip.

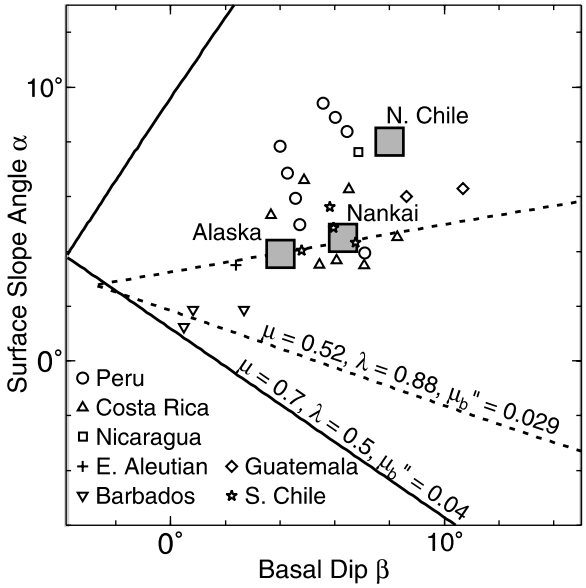

Figure 4. Surface slope angle versus basal dip for noncohesive wedges based on the classical Coulomb wedge theory. A pair of solid or dashed lines brackets a stable region for the shown set of material parameters. The top one of each pair represents extensionally critical states (on the verge of gravitational collapse), and the bottom one represents compressively critical states. The solid lines show the reference model, and the dashed lines show the weak wedge model of *Lallemand et al.* [1994]. Outer wedge geometries of the two prisms in Figure 2 and the northern Chile frontal prism discussed in section 5.5 are indicated by labeled large squares. Small symbols show prisms considered by *von Huene and Ranero* [2003].

[23] Most of the wedges in Figure 4 are nowhere near a compressively critical state for either wedge model. Except for Barbados, they all fall in the stable region of our reference model or in the extensionally unstable region of the weak wedge model. Because the structures of outer wedges or frontal prisms are not consistent with rapid collapse, the weak wedge model is not preferred. To produce the large surface slopes of these wedges with either the strong or weak critical wedge model, a much larger basal friction is needed. A key point of the expanded wedge theory, to be explained in section 4, is the recognition that higher basal friction and thus a compressively critical state can be achieved during great earthquakes.

[24] Outer or average wedge geometry for a number of margins has been explained using the classical wedge theory (Table 1), usually by assuming near-lithostatic λ

values. A high λ weakens the wedge material and, if combined with a strong basal fault, may allow a larger surface slope. Recent observations do not support the universal presence of near-lithostatic pore fluid pressures in submarine wedges [e.g., *Kukowski et al.*, 2001; *Kopp and Kukowski*, 2003; *Davis et al.*, 2006]. The once widely assumed high values of $\lambda > 0.9$ for the Barbados accretionary prism have not been substantiated by borehole observations [*Becker et al.*, 1997; *Foucher et al.*, 1997] and seismic velocity analyses which showed the wedge to be mostly hydrostatic except near and within the basal decollement [*Hayward et al.*, 2003]. A low or moderate long-term λ in the outer wedge is easier to understand than a high one, because pervasive active fracturing and faulting should enhance permeability. Using the expanded Coulomb wedge theory, we will show that lasting high overpressures are not required.

4. The Theory of Dynamic Coulomb Wedge

4.1. Elastic–Perfectly Coulomb Plastic Wedges

[25] In the classical theory, the wedge is perfectly Coulomb plastic. The Coulomb failure criterion defines a yield surface in the stress space, and solution (5) describes the state of stress on this yield surface. Beyond the yield surface, the wedge is unstable. Within the yield surface, the wedge is stable, but the stress is not defined because no constitutive relation has been specified for the stable regime.

[26] The most reasonable candidate for the constitutive relation of a stable wedge is that of linear elasticity. Assuming elastic behavior for the stable regime, we define an elastic–perfectly Coulomb plastic rheology for the wedge. The stress-strain relationship for this rheology is schematically illustrated in Figure 5. In the elastic loading phase leading up to failure (point A), stress increases linearly with strain, following the Hooke's law. When the stress reaches the yield envelope (point B), further deformation is perfectly plastic, and the stress stays constant, as represented by the flat line. This state (point B or B′) is described by the critical wedge solution of (5). Upon unloading, the wedge returns to the elastic state (e.g., point A′). The state of stress in the elastic regime depends on current boundary conditions only and is not affected by permanent deformation in the past, that is, stresses for points A and A′ are identical.

[27] Figure 5 also illustrates that for any critical wedge stress solution (B or B′) there must be an equivalent elastic solution, and that the elastic solution for a stable wedge (A or A′) must have a similar form to the elastic equivalence of the critical wedge solution. We present these elastic solutions in section 4.2.

4.2. Stress Solution for a Critical or Stable Wedge

[28] *Hu and Wang* [2006] obtained a general stress solution for an elastic wedge using the Airy stress function. The formulation of the problem is identical to that described by Figure 3 and equations (1) through (3), except that the basal normal traction in (2) needs to be explicitly specified using a constant gradient a,

$$\overline{\sigma}_n = \sigma_n + P = -a\rho g x \tan\theta \tag{10}$$

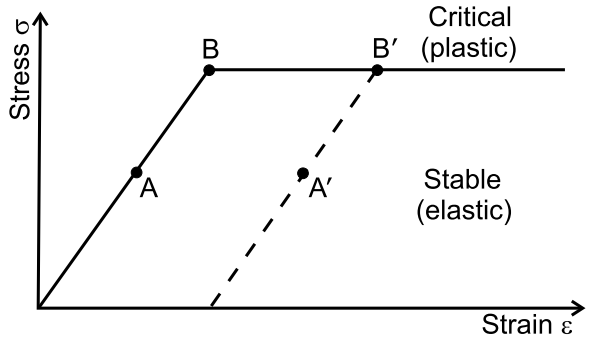

Figure 5. Schematic illustration of stress-strain relation for an elastic–perfectly plastic material. Points A and A′ are in the elastic regime. Despite a difference in permanent strain, they have an identical state of stress that can be described using an elastic solution. Points B and B′ are in the plastic regime (i.e., in a critical state). They also have an identical state of stress that can be described using either an elastic or a plastic solution.

In terms of effective stresses, their solution is

$$\overline{\sigma}_x = [k_2 + (1-\rho')\sin\alpha]\rho g x + (k_4 + \lambda\cos\alpha)\rho g y \tag{11a}$$

$$\overline{\sigma}_y = -(1-\lambda)\rho g y \cos\alpha \tag{11b}$$

$$\tau_{xy} = -k_2 \rho g y \tag{11c}$$

where

$$k_2 = \frac{(1-\lambda)\cos\alpha}{\tan\theta} - \frac{a\left(1-\mu_b'\tan\theta\right)}{\tan\theta} \tag{12a}$$

$$k_4 = -\frac{a}{\sin^2\theta} - \frac{3k_2}{\tan\theta} + \left[\frac{(1-\lambda)}{\tan^2\theta} - \lambda\right]\cos\alpha - \frac{(1-\rho')\sin\alpha}{\tan\theta} \tag{12b}$$

and $\theta = \alpha + \beta$. In the following, we show that a subset of this general solution is the solution for stable and critical wedges.

[29] We first show that if $\overline{\sigma}_x = 0$ at $y = 0$, the necessary condition for a wedge lacking surface cohesion, constant a is not an independent parameter but is determined by wedge geometry, pore fluid pressure, and basal friction. Using (11a), this condition gives

$$k_2 = -(1-\rho')\sin\alpha \tag{13}$$

(13) and (12a) lead to

$$a = \frac{(1-\rho')\tan\theta\sin\alpha + (1-\lambda)\cos\alpha}{1-\mu_b'\tan\theta} \tag{14}$$

Substituting (14) into (12b) and after some algebraic manipulation, we obtain

$$k_4 = -[m(1-\lambda)+\lambda]\cos\alpha \tag{15}$$

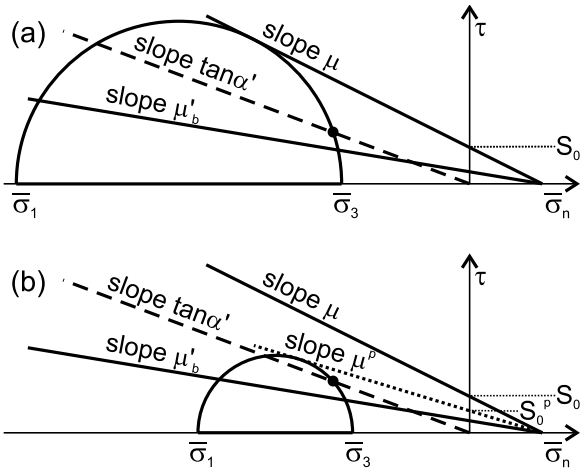

Figure 6. Mohr circles to illustrate the state of stress in critical and stable wedges with the same geometry and basal friction coefficient μ_b. (a) Stresses in a critically tapered Coulomb wedge. S_0 is cohesion, and μ is the coefficient of internal friction. (b) Stresses in a stable wedge. S_0^p is pseudocohesion and μ^p is the pseudocoefficient of internal friction. In both Figures 6a and 6b, the solid circle marks invariant point ($\overline{\sigma}_y$, τ_{xy}).

where

$$m = 1 + \frac{2\left(\tan\alpha' + \mu_b'\right)}{\sin 2\theta\left(1 - \mu_b' \tan\theta\right)} - \frac{2\tan\alpha'}{\tan\theta} \tag{16}$$

with α' defined in (8). Therefore the form of (11) that is applicable to a wedge lacking surface cohesion is

$$\overline{\sigma}_x = -m(1-\lambda)\rho g y \cos\alpha \tag{17a}$$

$$\overline{\sigma}_y = -(1-\lambda)\rho g y \cos\alpha \tag{17b}$$

$$\tau_{xy} = (1-\rho')\rho g y \sin\alpha \tag{17c}$$

[30] If $m = m^c$, (17) becomes identical with (5) and thus is the elastic equivalence of the critical wedge solution (points B and B′ in Figure 5). This means, for any critical wedge solution in the form of (5), we can always find an equivalent elastic solution for the same wedge geometry by equating (6) and (16). In the elastic equivalence, internal friction is no longer relevant; it is expressed in terms of other parameters through the relation $m = m^c$. If a Coulomb wedge exists for a given wedge geometry and strength, there are typically two m^c values corresponding to compressively and extensionally critical states, depending on basal friction μ_b''. If the value of m falls between the two m^c values, (17) represents the state of stress in a stable wedge (points A and A′ in Figure 5).

[31] The similarity between (17) and (5) is evident. They share all fundamental features. For example, just like in a critical wedge, the angle ψ_0 between σ_1 and the upper surface (Figure 3) in a stable wedge must be uniform, and, similar to (9), we must have

$$\alpha + \beta = \psi_b - \psi_0 \tag{18}$$

where ψ_b is the angle between σ_1 and the basal surface of the stable wedge (Figure 3). The physical meaning of this similarity can be made more intuitive by comparing Mohr circle illustrations of (5) and (17). Figure 6 represents states of stress in two wedges with identical geometry and basal friction angle φ_b. Figure 6a shows a critical state with cohesion S_0 defined in (4) and internal friction $\mu = \tan\varphi$, but Figure 6b shows a stable state. For the stable state, if we define a pseudocoefficient friction $\mu^p = \tan\varphi^p$ (dotted line tangential to the Mohr circle in Figure 6b), the two states in Figure 6 are completely analogous. Angle ψ_0 is thus determined from the following equation similar to (7)

$$\frac{\tan 2\psi_0}{\csc\varphi^p \sec 2\psi_0 - 1} = \frac{\tan\alpha'}{1+\eta} \tag{19}$$

One may be puzzled why the cohesion gradient η appears in the equation for an elastic wedge. In fact, the pseudocoefficient friction must be accompanied by a pseudocohesion S_0^p (Figure 6b). It can be shown that S_0^p has an identical form to S_0 as defined by (4), except that μ is replaced with μ^p, and therefore η here appears also as a pseudoparameter. By invoking φ^p, (16) can be written into a form similar to (6)

$$m = 1 + \frac{2(1+\eta)}{\csc\varphi^p \sec 2\psi_0 - 1} \tag{20}$$

If $\varphi^p = \varphi$, we have $\psi_0 = \psi_0^c$, $\psi_b = \psi_b^c$, and $m = m^c$. Using the Mohr circle, we readily obtain

$$\sin^2\varphi^p = \frac{(m-1)^2 + 4\tan^2\alpha'}{(2\eta + m + 1)^2} \tag{21}$$

[32] Expanding a well known example of *Dahlen* [1984], we demonstrate how stresses in a wedge of given geometry change elastically from one critical state to another in response to changing basal friction conditions (Figure 7). The hypothetical wedge is assumed to be noncohesive ($\eta = 0$) with $\beta = 4.2°$, $\alpha = 4°$, $\mu = 1.1$, and $\lambda = 0.8$. *Dahlen* [1984] has shown that this wedge is compressively critical if $\mu_b'' = 0.17$ (Figure 7a) but extensionally critical if μ_b'' is decreased to 0.017 (Figure 7e). Using (17), we have calculated stresses in stable wedges for three values of μ_b'' between the two critical values. If the angle between σ_1 and the upper surface $\psi_0 < 45°$, the wedge is compressively stable (Figure 7b). If $\psi_0 > 45°$, the wedge is extensionally stable (Figure 7d). If $\psi_0 = 45°$, it is in a neutral state (Figure 7c). The value of μ''_b at the neutral state, denoted μ''_{b-N}, is related to other parameters by

$$\mu''_{b-N} = \frac{(1-\lambda)\cos 2\theta}{\cot\alpha' + \sin 2\theta} \tag{22}$$

[33] The change of ψ_0 with μ_b'', referred to as the elastic stress path, for this wedge is shown in Figure 8a (thick solid

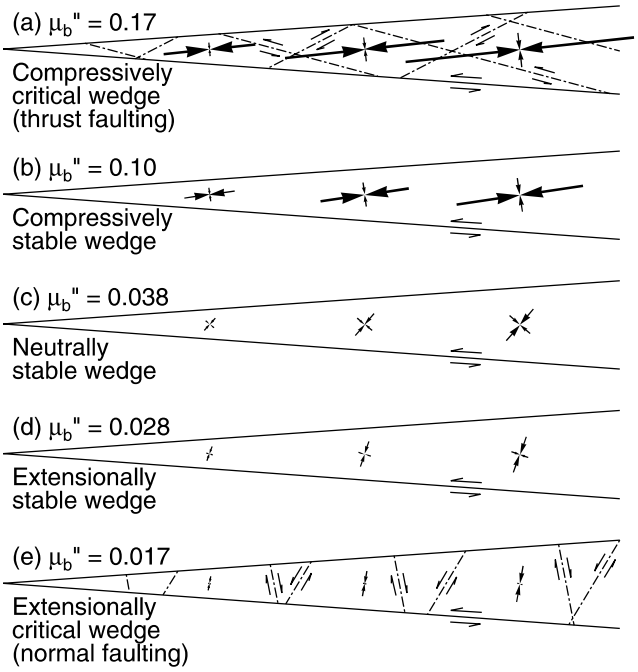

Figure 7. An example to show how stresses in an elastic–perfectly Coulomb plastic wedge, with $\alpha = 4°$, $\beta = 4.2°$, $\mu = 1.1$, and $\lambda = 0.8$, are affected by basal friction μ_b''. Converging arrows represent principal stresses, with the larger one being σ_1. (a) Compressively critical state. (b) Compressively stable state. (c) Neutral state (σ_1 is at 45° with the upper surface). (d) Extensionally stable state. (e) Extensionally critical state. In Figures 7a and 7e, dot-dashed lines are plastic slip lines.

line), together with stress paths for other surface slopes. For each geometry, ψ_0 changes between its two critical values corresponding to the two critical μ_b'' values. The end points of all curves (connected by a dashed line) outline the stable region. The $\alpha - \beta$ plot for the same wedge material but $\mu_b'' = 0.1$ is shown in Figure 8b, with the stable region "filled" with contours of ψ_0 determined using (20), in conjunction with (16) and (21). Figure 4 shows the leftmost portions of a plot similar to Figure 8b.

[34] Two special critical states are marked in Figure 8, featuring basal erosion (Figure 8a) and the angle of repose (Figure 8b), respectively. The angle of repose is the maximum value of α for the given set of material properties, reached in the extensionally critical state in which $\tan \alpha' = \mu$, that is, one the two conjugate sets of plastic slip lines becomes parallel with the upper surface. "Basal erosion" is often used as a generic term to indicate removal of materials from the underside of the wedge. Here it is used to indicate a specific compressively critical state in which $\mu_b'' = \mu(1 - \lambda)$, that is, one set of plastic slip lines in the critical wedge becomes parallel with the basal thrust [*Dahlen*, 1984]. At this μ_b'', no elastically stable surface slope exists.

4.3. Outer Wedges in Earthquake Cycles

[35] In this and the following sections, we treat the inner and outer wedges independently for simplicity. The state of stress in each of them is assumed to depend only on the basal stress directly beneath. The effects of ignoring stress interactions between the two parts will be discussed in section 4.5.

[36] We assume that the outer wedge of an accretionary prism overlies the velocity-strengthening part of the subduction fault where slip instability (earthquake nucleation) cannot occur. The actual coseismic behavior of the most updip part of subduction faults has never been directly observed, but studies of tsunamis and seismic waves generated by great earthquakes all seem to indicate that subduction faults do not rupture all the way to the toe of the wedge [*Wells et al.*, 2003]. Various models have been proposed to explain the velocity-strengthening behavior of the updip segment, such as low strength of the poorly consolidated sediments [*Byrne et al.*, 1988], presence of slippery minerals [*Hyndman and Wang*, 1993], and a combination of diagenetic, metamorphic, and hydrological conditions [*Moore and Saffer*, 2001].

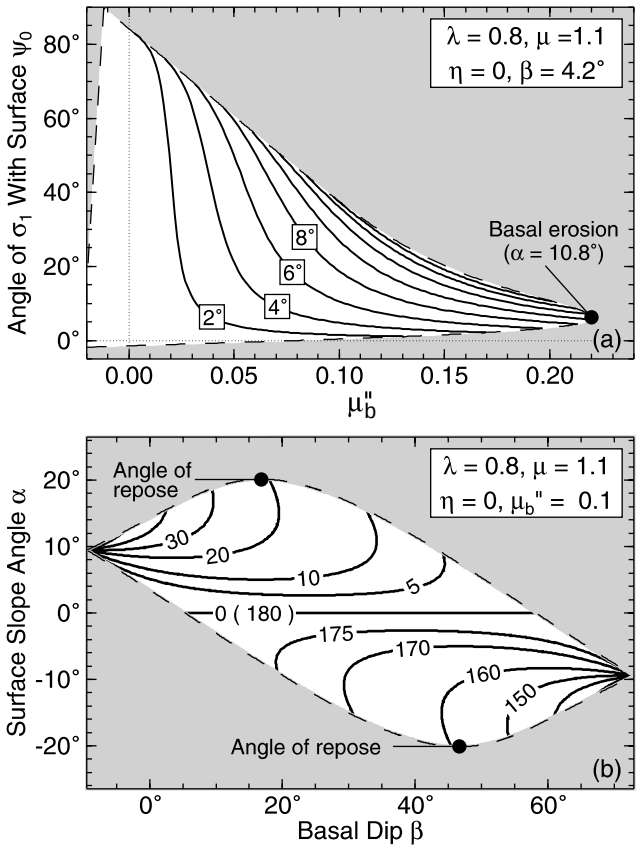

Figure 8. (a) Plot of the angle of σ_1 with the upper surface ψ_0 (defined in Figure 3) versus basal friction μ_b'' (the elastic stress path) for the wedge in Figure 7 ($\alpha = 4°$) and similar wedges but with different surface slopes. Each stress path is terminated at the extensionally critical state at a lower μ_b'' and the compressively critical state at a higher μ_b''. The end points (connected by a dashed line) outline the stable region for the given β value (= 4.2°) in the $\psi_0 - \mu_b''$ space. (b) Plot of α versus β for the same wedge material with $\mu_b'' = 0.1$, with ψ_0 contours (in degrees) in the stable region encompassed by the line of critical states (dashed line). In both Figures 8a and 8b, the unstable region is shaded.

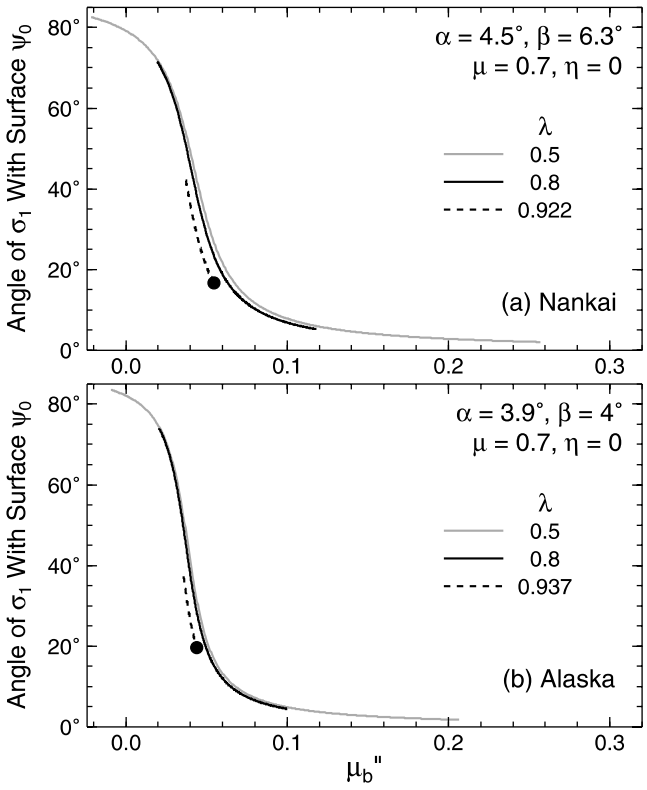

Figure 9. Elastic stress paths for the outer wedges of the two prisms in Figure 2 with $\mu = 0.7$, $\eta = 0$. Solid circle marks the state of basal erosion.

[37] Velocity strengthening implies that μ_b'' decreases with decreasing slip rate. In the later part of an interseismic period long after a previous earthquake, the updip segment is "protected" by the locking of the seismogenic part of the fault further downdip. If this updip segment has little slip, μ_b'' is expected to be low, e.g., around the reference value of 0.04 or lower. Stress paths for the two outer wedges of Figure 2 with $\mu = 0.7$ are shown in Figure 9 for a few λ values. In most of the interseismic period, they are expected to be in the stable regime (point A or A′ in Figure 5) for a wide range of μ_b'' and λ values.

[38] During an earthquake, as the updip segment of the fault is forced to slip, it suddenly becomes stronger. The increase in μ_b'' may be due to the intrinsically velocity-strengthening nature of μ_b and perhaps also a decrease in fault zone fluid pressure. The outer wedge is elastically compressed at the beginning of the coseismic slip. If μ_b'' increases to the end of the elastic stress path (Figure 9), the wedge enters a critical state and compressive failure occurs (point B or B′ in Figure 5). If the earthquake is too small to push the outer wedge into the critical state, the wedge simply experiences a brief phase of elastic compression.

[39] After the earthquake, when the seismogenic part of the fault is locked, the updip velocity-strengthening segment is expected to creep to relax the coseismically generated stress in the outer wedge. Any relaxation immediately brings a critical wedge back to the stable elastic regime.

[40] If λ stays constant in this cycle, wedge stress simply moves back and forth along one stress path (Figure 9). However, pore fluid pressure within the wedge must increase during coseismic compression of the wedge and decrease afterward. A proper treatment of the fluid pressure pulse in an elastic wedge requires the theory of poroelasticity, and λ must be stress-dependent. For example, for elastic coseismic deformation, in which the system can usually be assumed to be undrained, $P = \gamma(\Delta\sigma_x + \Delta\sigma_y + \Delta\sigma_z)/3$, where γ is the (three-dimensional) loading efficiency (or the Skempton coefficient) [*Wang*, 2004], and $\Delta\sigma_i$ ($i = x, y, z$) is incremental stress in the fluid-solid mixture. In order to obtain the exact stress solution of (17), we have to assume a constant λ. However, on the basis of this simple solution we may qualitatively predict the effect of fluid pressure variation: During an earthquake, wedge stress should move on to stress paths for higher λ values (Figure 9). For a higher λ, the critical state is reached at a lower μ_b''. After the earthquake, wedge stress should gradually move to stress paths for lower λ values because of stress relaxation and fluid drainage. The fluid cycle will be further discussed in section 5.4.

[41] Figure 10 shows how the critical value of μ_b'' depends on λ. This plot also shows the sensitivity of the results to the choice of internal friction μ and cohesion gradient η. For each μ or η, there are two branches of μ_b'' as a function of λ encompassing the stable region, with the upper branch for compressively and lower branch for extensionally critical states, respectively. Greater pore fluid pressure makes the wedge weaker, so that compressive failure can occur at a lower basal friction, and gravitational collapse can occur at a higher basal friction.

[42] Coseismic increase in λ can also provide the condition for basal erosion. The state of basal erosion (defined at the end of section 4.2) requires not only a high enough μ_b'', but also a high λ. For $\mu = 0.7$, basal erosion for our Nankai cross section requires $\lambda = 0.92$ (Figures 9a). Although this is unlikely to happen for the whole Nankai outer wedge, it may locally occur just above the basal decollement during an earthquake.

[43] In summary, we propose that sediment accretion, permanent outer wedge deformation, and limited basal erosion, take place mainly during great earthquakes, and observed surface slope of an outer wedge is determined by the peak value of μ_b'' reached at the time of the largest

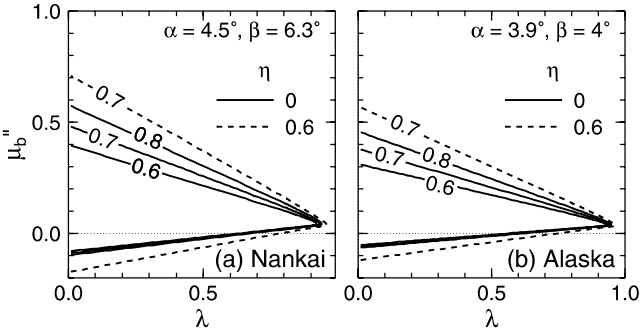

Figure 10. Critical values of basal μ_b'' as a function of pore fluid pressure ratio λ for the Nankai and Alaska outer wedges with different internal frictions μ (labeled on each curve). (a) Nankai outer wedge. (b) Alaska outer wedge.

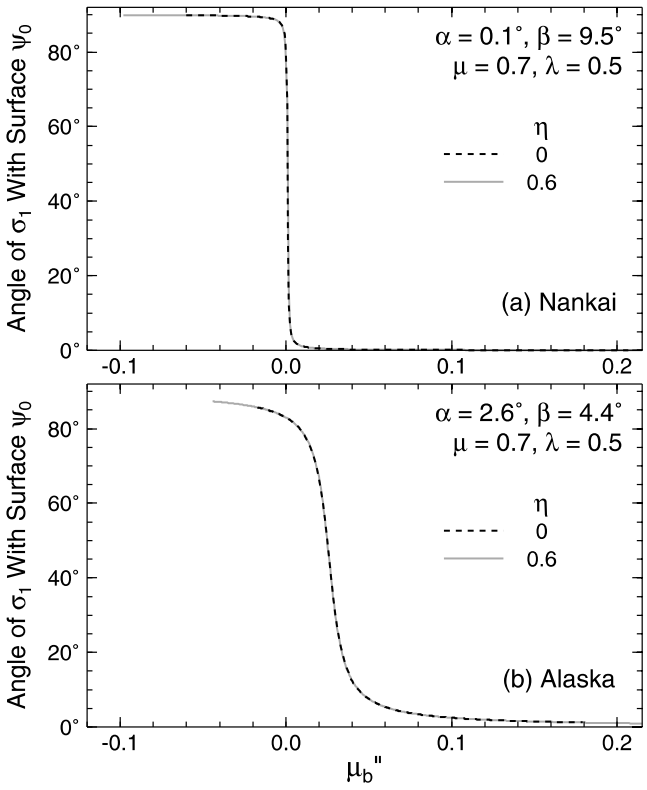

Figure 11. Elastic stress paths for the inner wedges of the two prisms in Figure 2, with $\mu = 0.7$, $\lambda = 0.5$.

earthquakes, not by the reference μ_b'' value assumed for Figure 4.

4.4. Inner Wedge in Earthquake Cycles

[44] We postulate that the inner wedge overlies the stick-slip, i.e., velocity-weakening, part of the subduction fault: the seismogenic zone. In our conceptual model, we only consider the core region of the seismogenic zone. The transition from the updip velocity-strengthening segment to this core region awaits more detailed future studies. The downdip limit of the seismogenic zone [*Hyndman and Wang*, 1993; *Peacock and Hyndman*, 1999] is less important to the subject of this study.

[45] In the end-member scenario we are considering, the stick-slip segment of the subduction fault is in a locked state or slips extremely slowly in the interseismic period. The peak shear stress that the fault can sustain is probably represented by low μ_b'' values such as 0.04 discussed in section 3.2. Because the subduction fault fails (and ruptures) at such a low μ_b'', the inner wedge never comes close to compressive failure. This explains the general lack of recent contractile structure in inner wedges. Stress paths of the two inner wedges of Figure 2 for $\lambda = 0.5$ are shown in Figure 11. We include models with $\eta = 0.6$ to account for the possible greater strength of inner wedges than outer wedges. A greater η makes it more difficult to cause Coulomb failure (i.e., the wedge is stable over a wider range of μ_b'') but does not affect the shape of elastic stress paths. The exact interseismic μ_b'' value is obviously unimportant in keeping the inner wedge in the stable regime, because the stability occurs over a very wide range of μ_b'' values.

[46] Because of the velocity-weakening nature of the seismogenic zone, μ_b'' decreases during a great earthquake, and the wedge follows the stress path in the direction toward low μ_b'' and high ψ_0, opposite of the coseismic behavior of the outer wedge, and the wedge becomes less compressive.

[47] Even the weakest inner wedge assumed ($\eta = 0$) stays in the stable regime throughout great earthquake cycles (Figure 11). The inner wedge thus provides a stable environment for the formation of forearc sedimentary basins, which explains the correlation between the downdip positioning of megathrust rupture with the location of forearc basins observed at many accretionary margins [*Wells et al.*, 2003]. *Wells et al.* [2003] noticed that the second-order, along-strike positioning of patches of greater coseismic fault slip also seems to correlate with the location of forearc basins. The mechanism for this correlation, if confirmed, deserves further study, and the key question may be about what leads to the anomalous areas between basins. The stability of the inner wedge also helps explain the presence of an apparent "dynamic backstop" landward of the outer wedge [*Kopp and Kukowski*, 2003]. In addition to a landward increase in consolidation state of wedge sediments, the seismogenic behavior of the subduction fault can cause a change in structural style and even a surface slope break around the outer-inner wedge transition. In fact, the stable environment of the inner wedge should facilitate consolidation.

[48] The case of $\mu_b'' = 0$, i.e., zero shear stress, represents complete stress drop of the seismogenic zone during an earthquake. It is theoretically possible to cause extensional failure by coseismically raising λ to 0.99 and 0.69 for Nankai and Alaska inner wedges, respectively, although we think near-lithostatic fluid pressures are very unlikely. Of course, the applicability of the wedge model decreases as we go landward, because the rheology of the deeper region may increasingly deviate from Coulomb.

4.5. An Illustration of the Stress Cycle

[49] Using the geometry of the Nankai cross section off Kii Peninsula (Figure 2a), we illustrate a possible stress evolution history of an accretionary margin, including both outer and inner wedges, throughout a great earthquake cycle (Figure 12). We also use this illustration to highlight some important issues that require future observations. As explained in section 4.3, a stress-dependent λ cannot be dealt with by our analytical solution, and therefore we assign λ values to different stages of the stress evolution. As mentioned above, the outer and inner wedges have been treated as two independent wedges. In reality, there is stress transfer between the two parts. For example, the state of stress in the inner wedge depends not only on the shear stress of the megathrust seismogenic zone directly beneath, but also on stresses in the outer wedge. By ignoring the interaction between the two parts, we assume the length of the transitional segment between them (dashed outlines) is at least a couple of times its thickness. In the following description of the stress cycle illustration in Figure 12, we will briefly point out the effects of ignoring this interaction.

[50] The degree of compressiveness in a wedge, represented by the orientation of σ_1, is controlled by basal friction. Therefore temporal variations of basal friction in the updip and seismogenic segments of the plate interface,

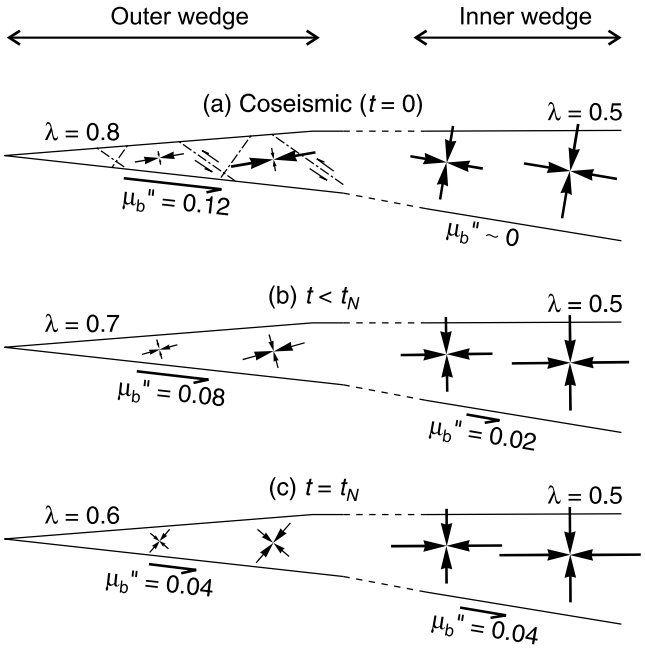

Figure 12. An illustration of stress cycle using the geometry of the Nankai prism off Kii Peninsula. The λ values have been assumed for illustration purpose to reflect the evolution of pore fluid pressures in the stress cycle. The state of stress in the transitional segment between the outer and inner wedges (dashed outlines) cannot be modeled using equation (17), and therefore the pairing up of μ_b'' values beneath the outer and inner wedges is assumed. (a) Coseismic. The outer wedge is in a critical state; μ_b'' reaches its peak value beneath the outer wedge and minimum value beneath the inner wedge for their assumed λ values. (b) Postseismic. The outer wedge begins to relax, but the inner wedge is compressed because of the locking of the seismogenic zone beneath it. (c) Interseismic at $t = t_N$. The outer wedge is in a neutral state. Shear stress in the seismogenic zone beneath the inner wedge approaches fault strength.

as schematically illustrated in Figure 1c, also portrays how the compressiveness of the outer and inner wedges, respectively, changes with time.

[51] During a great earthquake, the outer wedge is pushed into the compressively critical state, and σ_1 is subhorizontal (Figure 12a). For this illustration, coseismic strain is assumed to have caused moderately high overpressure in the outer wedge ($\lambda = 0.8$), and the peak μ_b'' value of the updip velocity-strengthening fault segment is therefore 0.12 (also see Figure 9a). On the other hand, on the seismogenic zone, the shear stress is assumed to have dropped to zero, modeled using $\mu_b'' = 0$. The inner wedge is thus in an extensionally stable state (Figure 12a). We expect the coseismic process to take minutes to complete, but future observations will help constrain the timescale. If the interaction between outer and inner wedges were included, horizontal compression would presumably decrease gradually landward across the transitional segment, and the most seaward part of the inner wedge would be less extensional than shown here.

[52] After the earthquake, the outer wedge begins to relax because of the decrease in μ_b'', but the inner wedge begins to become more compressive because of the locking of the seismogenic zone beneath it (Figure 12b). They both stay in the stable regime over the interseismic period. Stress relaxation in the outer wedge and the transitional segment is expected to be accompanied with some seaward motion of the outer wedge. By analogy with the shallow velocity-strengthening part of a strike-slip fault, postseismic shear stress decrease in the updip segment of the subduction fault may follow a logarithmic form [*Marone et al.*, 1991]. The rate of the stress relaxation is an important subject for future research.

[53] To facilitate discussions, we define an outer wedge relaxation time t_N, the time required for μ_b'' to decrease from its coseismic peak value to μ_{b-N}'' (see Equation (22)). At this time, the outer wedge is in a neutral state (Figure 12c). As the stress relaxes, pore fluid pressure in the outer wedge decreases, depending also on the rate of drainage. For illustration purpose, we arbitrarily assume a $\lambda = 0.6$ for the neutral state. With this λ value, the value of μ_{b-N}'' for the Nankai profile happens to be the reference μ_b'' value of 0.04.

[54] Theoretically, if μ_b'' decreases to a very small value at a rate faster than that of fluid pressure decrease, an outer wedge may become extensionally critical (gravitational collapse) (Figure 9). For both margins in Figure 2, extensional failure could occur at $\mu_b'' = 0.02$ if $\lambda = 0.8$. The fact that normal faulting is not observed in these outer wedges indicates that μ_b'' may never decrease to such a small value or that the fluid pressure may decrease faster. We will know only from future observations whether μ_b'' can become small enough to allow the wedge to be more extensional than a neutral state shown in Figure 12c. Nevertheless, relaxation may contribute to the pristine normal faulting [(section 3.2)] in the area of inner-outer wedge transition (Figure 2a), where the presence of the slope break precludes a quantitative analysis using the uniform wedge model.

[55] Over the interseismic period, shear stress along the locked zone of the subduction fault will gradually increase. Therefore near the end of the period, compression in the inner wedge increases to its maximum, modeled using the reference value of $\mu_b'' = 0.04$. Although not illustrated in Figure 12, it is likely that pore fluid pressure in the inner wedge also varies significantly throughout the stress cycle.

[56] In this illustration, we have ignored transient fault motion between great earthquakes and other causes for stress variations. Aseismic slip of different parts of subduction faults has been geodetically detected for a number of subduction zones including Nankai [*Ozawa et al.*, 2002] and Alaska [*Freymueller et al.*, 2001]. It is not clear whether parts of the locked seismogenic zone at these two margins actually slip aseismically from time to time. It they do, pulses of compression may occur in the outer wedge. Earthquakes in the subducting slab and continental crust may also cause stress changes in the accretionary wedge. Real subduction zones are not two-dimensional, and fault seismogenic behavior and wedge geometry vary along strike (Figure 1a). Anomalous structural features such as subducting seamounts may inhibit rupture propagation. Different segments may rupture at different times and, even in the same earthquake, may slip by different amounts.

These complications should be respected when the dynamic wedge theory is applied.

5. Discussions

5.1. Updip Limit of the Seismogenic Zone

[57] In presenting the above theory, we have assumed that the updip limit of the seismogenic zone controls the transition from the outer wedge to the inner wedge and therefore is located in the area of an abrupt change in structural style and surface slope. It is important to recognize that although the most seaward part of the inner wedge may not be strong in terms of Coulomb yield strength, e.g., its internal friction may be low, it is capable of storing elastic strain energy within its stable regime and thus contributing to earthquake nucleation and rupture.

[58] The updip limit of the seismogenic zone must be transitional. Coseismic slip decreases from a finite value to zero over some distance. We do no know which point within this distance range should be defined as the seismogenic limit. The change from updip velocity strengthening to downdip velocity weakening may be controlled by a range of thermal, hydrological, and mineralogical processes [*Moore and Saffer*, 2001], but temperature seems to be an indirect but dominant factor [e.g., *Oleskevich et al.*, 1999; *Currie et al.*, 2002]. Such a change may also be gradational and may involve a zone of conditional stability [*Scholz*, 2003]. Although we cannot pinpoint the exact position of the updip limit because of these uncertainties and also because of uncertainties about the behavior of the transitional wedge segment between inner and outer wedges as discussed in section 4.5, the dynamic wedge concept, after "calibration" against field observations, potentially provides a practical means to constrain approximately this limit using structural and bathymetric observations.

[59] Of some interest is the distinctness of the slope break. The break is rather distinct for the Nankai profile (Figure 2a) but much less distinct for the Alaska profile (Figure 2b). In the absence of other complications such as subducting seamounts, the distinctness may depend on the sharpness of the updip limit of the seismogenic zone. Rupture of the subduction fault at Nankai off Kii Peninsula may tend to terminate rather sharply near the slope break, but rupture along the Alaska profile may terminate much more gradually or stop at different distances from the trench in different great earthquakes. A margin-parallel fault to the west of the Alaska profile of Figure 2b slipped during the 1964 great earthquake [*Plafker*, 1972]. This fault is located within what we call the inner wedge on the basis of Figure 2b, but its geometry at depth is yet to be constrained by seismic imaging. If it indeed is a contractile out-of-sequence thrust fault, its activation indicates coseismic inner wedge compression unlike what is portrayed in the idealized illustration of Figure 12a, and for this location the fault area of greatest stress drop during the 1964 event has to be further downdip.

5.2. Evolution of Wedge Geometry

[60] For the outer wedge, we have reasoned [(section 4.3)] that the surface slope is determined by the peak basal stress achieved in large earthquakes. With all other conditions assumed to be the same, if a large earthquake causes the basal stress to rise to an unprecedented level, the wedge will enter the compressively unstable regime, beyond the high-μ_b'' end of the stress paths defined for the current wedge geometry. In this case, the wedge must deform in order to attain a greater slope angle. If such a large earthquake is a rare event, it may generate irregular seafloor topography but not a new average slope angle. If events of similar size continue to occur, then the greater surface slope will be established over many earthquake cycles. Smaller events that do not raise the basal stress to the peak value cause elastic deformation in the wedge, or local permanent deformation in heterogeneous wedges of the real world, but will not control the slope angle.

[61] Unless all sediment on the incoming plate is subducted, accretion at the toe must occur after some plate convergence, even if the outer wedge stays in the stable regime over a number of earthquake cycles. It is important to recognize that details of deformation around the toe are not readily modeled using a wedge theory. Seaward growth of the wedge by accretion involves generating new frontal thrusts in the nearly flat-lying incoming sediment formation under lateral compression [*Schott and Koyi*, 2001]. Initial deformation of the sediment formation may give rise to an ephemeral protowedge with a shape different from that of the outer wedge.

[62] Because the inner wedge generally stays in the stable regime, as we have shown in section 4.4, how it has evolved to the present shape cannot be modeled by using a critical wedge theory alone. For margins dominated by subduction erosion, a model of evolution has been proposed by *von Huene et al.* [2004]. For accretionary margins where the inner forearc partially consists of older accreted sediments, we may speculate on the following scenario.

[63] We envision that the long-term growth of the accretionary prism and seaward migration of the trench relative to the volcanic arc will eventually cause the updip limit of the seismogenic zone also to move seaward. Consequently, the most landward part of the former outer wedge no longer overlies the updip velocity-strengthening segment of the megathrust. In the process of incorporating this newly stabilized part into the inner wedge, one or a combination of two processes may happen. First, limited basal erosion of the outer wedge during great earthquakes [(section 4.3)] may transport sediment downdip. Along the Nankai profile (Figure 2a), underplating of this material has contributed to a slight landward tilt of the inner wedge as reflected by the gentle dip of the forearc basin strata [*Park et al.*, 2002]. Second, seaward migration of the trench must be accompanied with a slight rolling back and/or flattening of the subducting slab, causing subsidence and allowing more sediment to be deposited in forearc basins [*McIntosh et al.*, 2006]. For exceedingly fast wedge growth such as at the northern Cascadia subduction zone, the seaward migration of the deformation front and the sesimogenic zone may be too fast for the wedge geometry to keep up, and part of the seismogenic zone may currently underlie the outer wedge.

5.3. Activation of Splay Faults and Tsunami Generation

[64] During a great earthquake, σ_1 in the outer wedge is predicted to be subhorizontal (Figure 12a). Thrust motion of splay faults under this condition may constitute an impor-

tant mode of wedge deformation. The dynamic Coulomb wedge theory thus supports *Park et al.*'s [2002] hypothesis of coseismic activation of splay faults at Nankai. Well after an earthquake, when the wedge is somewhat relaxed (Figure 12c), the splay faults become more stable.

[65] Unlike the inner wedge process of gradual accumulation of elastic strain energy followed by a coseismic release, energy is both accumulated and partially released in the outer wedge during one great earthquake. Work done coseismically by the inner wedge on the outer wedge is instantaneously converted into elastic strain energy in the outer wedge. During this time, stress in the elastic outer wedge quickly moves to the high-μ_b'' end of stress paths (Figure 9). When failure stress is reached at the peak basal friction value, splay faults slip to release the strain energy accumulated just a moment before. Whether they slip in the form of violent seismic rupture or more slowly depends on their own frictional behavior.

[66] Again, it is important to recognize that the weak materials of the outer wedge are capable of storing elastic strain energy in its stable regime and therefore actively participating in the rupture of splay faults. Real submarine wedges are probably not perfectly plastic as represented by the horizontal straight line in Figure 5, and a brief phase of strain hardening may precede failure. This will allow more elastic strain energy to be accumulated in the wedge before splay fault rupture. The prediction that splay faults are activated during great earthquakes will be tested by planned drilling into the megasplay fault shown in Figure 2a.

[67] Coseismic slip of splay faults amplifies the vertical component of megathrust slip and hence seafloor uplift, facilitating tsunami generation. Splay faulting is suspected to have contributed to tsunami generation in the 1946 Nankai earthquake [*Cummins and Kaneda*, 2000]. Seafloor observations right after the 2004 Sumatra earthquake ($M_w > 9$) suggest that splay faulting played an important role in its tsunami generation (K. Suyehiro, personal communication, 2005). Sudden, rapid splay fault motion and permanent wedge deformation during an earthquake will also increase the ruggedness of the seafloor, with locally unstable structures inductive to mass wasting, contributing to tsunami generation. Note that here we only emphasize how splay faulting and wedge failure may *enhance* tsunami generation. Implications of the wedge theory for understanding the main cause of tsunami, i.e., coseismic seafloor uplift due to elastic deformation, will be discussed elsewhere.

[68] *Ito and Obara* [2006] reported transient clusters of very low frequency earthquakes off the Nankai coast that occurred over the past few years. They proposed that these events are mostly within the outer accretionary wedge and represent thrust motion of out-of-sequence faults. The triggering mechanism for these events is presently not understood. They may be associated with episodic aseismic motion of the megathrust seismogenic zone that causes pulses of compression in the outer wedge. The close association of one cluster with a recent major earthquake within the subducting plate near the trench suggests that slab dynamics may play an important role [*Obara and Ito*, 2005]. Regardless of the triggering mechanism, if these events truly represent the activation of thrust faults, they indicate that parts of the outer wedge are currently in a near-critical stable state so that failure can occur upon small perturbation. That is, several decades after the 1944 great earthquake, the outer wedge may still be in a state between what is shown in Figures 12a and 12b. Whether this indicates that t_N is very long or that other processes, such as incomplete locking of the seismogenic zone or elastic shortening of the subducting plate beneath the outer wedge, are causing prolonged compression of the outer wedge deserves further research.

5.4. Fluid Cycle

[69] It has been recognized that transient models of hydrogeology of submarine wedges are needed to explain many observations [*Bekins and Screaton*, 2006]. The idea of earthquake-modulated fluid cycles has existed for a long time [e.g., *Sibson*, 1981]. Such a fluid cycle is an important component of the dynamic wedge theory.

[70] The dynamic wedge theory postulates that pore fluid pressure in the outer wedge should increase during a great earthquake but decrease afterward. The timescale of the postseismic decrease depends on a few factors. First, it depends on the permeability structure and thus the rate of drainage. The timescale for this process is characterized by the hydraulic diffusion time constant $t_d = L^2/d$, where L is a length scale (e.g., wedge thickness) and d is the hydraulic diffusivity. Second, it depends on the rate of stress relaxation, which in turn is controlled by the friction properties of the portion of the subduction fault beneath the outer wedge. The timescale of the stress relaxation is characterized by t_N as discussed in section 4.5. Third, it may depend on an independent source of fluid pressure, namely fluid production by such processes as mineral dehydration reactions in wedge sediments [*Moore and Vrolijk*, 1992]. Recent observations in an instrumented borehole near the toe of the Nankai outer wedge (about 200 km west of the profile shown in Figure 2a) show a background gradual decrease in the fluid pressure [*Davis et al.*, 2006]. This observation suggests that the fluid pressure may still be decreasing six decades after the 1946 great earthquake in that area. The borehole monitoring also recorded a pressure pulse in temporal and spatial correlation with one of the clusters of very low frequency events reported by *Ito and Obara* [2006] and discussed in section 5.3. The pressure pulse may indicate transient aseismic motion of a part of the locked seismogenic zone or dynamics of the incoming plate [*Davis et al.*, 2006].

[71] The fluid cycle may also modulate gas hydrate formation and seafloor biosystems. Transportation of organic carbon and formation of methane hydrates are strongly related with fluid migration [*Hyndman and Davis*, 1992]. The fluid regime should be the most active during and following great earthquakes. Splay faulting and other types of wedge deformation during earthquakes perturb the thermal field and may cause local dissociation of hydrates, adding nutrients to pore fluids. Shortly after the earthquake, there should be abundant discharge of nutrient-bearing fluids to support seafloor biocommunities in places like cold seeps. With the decrease in overpressures and thus fluid discharge, the communities may diminish.

5.5. Frontal Prisms of Erosion-Dominated Margins

[72] At margins dominated by subduction erosion, the outer wedge is composed mainly of rock framework of the

upper plate, but its most seaward portion is a small frontal prism consisting of slump debris derived from land and perhaps some accreted seafloor sediments [*von Huene et al.*, 2004]. Here we use the northern Chile margin (Figure 13a) as an example to point out differences between these frontal prisms and outer accretionary wedges. Details of the geological structure and the seismic data used to constrain the structure are described by *von Huene and Ranero* [2003] and *Sallarès and Ranero* [2005]. Situations along the Peru and northeast Japan margins are similar to northern Chile [*von Huene and Lallemand*, 1990]. The surface slope of frontal prisms is usually much steeper than that of outer accretionary wedges as shown in Figure 2.

[73] One difference from a typical outer accretionary wedge is that the frontal prism has a true crystalline backstop that gives rise to a slope break (Figure 13a), although the backstop may be fractured. The second difference is that the frontal prism and much of its backstop both overlie the updip velocity-strengthening segment of the subduction fault, and thus the frontal prism and its backstop together form the outer wedge. The seismogenic zone is further downdip, and therefore the inner wedge is located further landward. The rupture of the magnitude 8 Antofagasta megathrust earthquake of 1995 at this location started from a depth of about 44 km and propagated updip to around 20 km depth [*Husen et al.*, 2000]. The third difference is that the frontal prism is experiencing active basal erosion. Removal of sediments from the underside of the prism must be in a dynamic equilibrium with deposition and accretion to keep the prism at a small size [*von Huene et al.*, 2004]. Sediment recycling makes the prism more pervasively fractured and less consolidated than outer accretionary wedges. Despite these differences, the frontal prism is expected to be similar to outer accretionary wedges in switching between stable and critical states in earthquake cycles.

[74] Figure 13b shows suggested elastic stress paths for the northern Chile frontal prism. For the pervasively fractured and poorly consolidated small prism, the average value of the internal friction should be close to that of the incoming sediment. *Adam and Reuther* [2000] used a μ = 0.7 when applying the classical theory to this frontal prism. We follow *von Huene and Ranero* [2003] to assume μ = 0.51, but the exact value is unimportant for the purpose of illustrating the concept. Also because of the pervasive fracturing, fluid pressure in the prism is expected to be lower than in outer accretionary wedges in both interseismic and coseismic phases. For the geometry of the northern Chile frontal prism, the state of basal erosion $\mu_b'' = \mu(1 - \lambda)$ occurs at λ = 0.84 and μ_b'' = 0.09. We propose that these values are achieved during great earthquakes when the prism is suddenly pushed to move forward by its crystalline backstop which is in turn triggered to move by the rupture of the seismogenic zone further downdip. It is these values that determine the surface slope of the frontal prism. The λ and μ_b'' of the frontal prism are expected to be lower during the period between large earthquakes when the seismogenic zone is either locked, as is currently the situation off Peru [*Gagnon et al.*, 2005], or slipping very slowly, as in parts of the Japan Trench [e.g., *Uchida et al.*, 2003].

[75] The state of basal erosion is fundamental to the frontal prism not only for helping balance sediment budget.

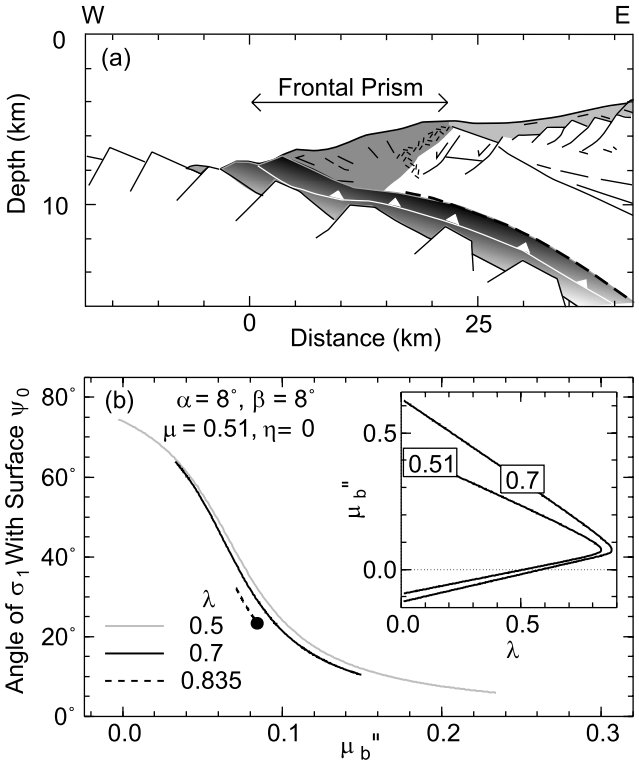

Figure 13. (a) Cross section of the frontal part of the northern Chile margin based on the work by *Sallarès and Ranero* [2005]. The portion of the upper plate shown here, including the frontal prism and its backstop, all belongs to what we refer to as the outer wedge. (b) Elastic stress paths for the northern Chile frontal prism assuming $\mu = 0.51$ and $\eta = 0$. Solid circle marks the state of basal erosion. The inset shows the critical values of basal μ_b'' as a function of pore fluid pressure ratio λ for two different internal frictions $\mu = 0.51$ and 0.7 and $\eta = 0$.

As emphasized by *von Huene and Ranero* [2003], one should not be misled by the graphical horst-and-graben structures of the subducting slab to envision a strong interplate friction. These structures are leveled by sediments. Because the ultimate coseismic strength of the fault μ_b'' is the strength of the wedge material $\mu(1 - \lambda)$, the plate interface must be a shear zone such that the decollement is not distinctly defined.

6. Conclusions

[76] We have expanded the classical Coulomb wedge theory for accretionary prisms by considering temporal variations of stresses along the megathrust fault and within the wedge in great earthquake cycles. The new theory consists of two key components: (1) the postulation that the actively deforming outer wedge and the much more stable inner wedge overlie the updip velocity-strengthening portion and the downdip seismogenic zone of the subduction fault, respectively, and (2) an exact stress solution for an elastic–perfectly Coulomb plastic wedge. The solution reproduces exact critical stress solutions for noncohesive [*Dahlen*, 1984] and cohesive [*Zhao et al.*, 1986] Coulomb

wedges in the classical theory and provides expressions for stresses in stable wedges.

[77] The new theory explains that for the end-member scenario in which the seismogenic zone alternates between interseismic locking and coseismic slip, the outer wedge switches between stable and critical states in earthquake cycles, with its topography controlled by the peak strength of the updip velocity-strengthening segment of the subduction fault. The outer wedge enters the critical state during great subduction earthquakes, when sediment accretion, basal erosion, and activation of splay faults take place. Between earthquakes, stresses in the outer wedge relax. The inner wedge remains mostly in the stable regime throughout the earthquake cycles.

[78] The theory offers first-order explanations for some important observations, such as the sharp contrast in structural style between inner and outer wedges, often accompanied with a surface slope break, the coexistence of a relatively large outer wedge surface slope and a very weak subduction fault, and the correlation between the locations of megathrust rupture zones and forearc basins. The theory does not require the presence of long-lasting exceedingly high pore fluid pressures within the wedge. We have demonstrated that the mechanics of outer wedges can be explained if fluid pressure is elevated during great earthquakes, coseismically weakening the wedge material, even if the pressure may be lower prior to the earthquake.

[79] The theory potentially provides a conceptual framework for investigating the position of the seaward limit of the megathrust seismogenic zone, the evolution history of accretionary prisms and forearc basins, splay-faulting during great earthquakes and its role in accommodating deformation and generating tsunami, and the variation of wedge fluid regime throughout earthquake cycles. It also provides a theoretical basis and a mechanism for the active basal erosion of frontal prisms at margins dominated by subduction erosion.

[80] **Note added in proof.** Just before we received page proofs for this manuscript, we became aware of a paper by *Hsu et al.* [2006] reporting an important finding after the *M*8.7, 28 March 2005 Nias-Simeulue earthquake at the Sumatra subduction zone. Hsu et al. showed that an updip segment of the subduction fault, beneath the outer wedge, did not rupture at the time of the earthquake but exhibited significant after slip logarithmically decreasing with time. For the first time, deformation observations were made close enough to the trench and had sufficient resolution to constrain coseismic and postseismic behavior of the updip segment. This finding strongly supports the prediction of the dynamic Coulomb wedge theory such as described in paragraphs 38, 39, and 52 of our paper.

[81] **Acknowledgments.** T. Brocher, E. Davis, N. Kukowski, J. C. Moore, R. von Huene, D. Scholl, and R. Wells read original versions of the manuscript and provided numerous insightful comments and suggestions. Discussions with them and with J. He, R. D. Hyndman, Y. Ito, G. Kimura, C. Marone, and K. Obara helped clarify many issues and concepts. Reviews by S. Gulick, K. Brown, and G. Moore further improved the paper. Geological Survey of Canada contribution 2005721.

References

Adam, J., and C. D. Reuther (2000), Crustal dynamics and active fault mechanics during subduction erosion: Application of frictional wedge analysis on to the North Chilean Forearc, *Tectonophysics*, *321*, 297–325.

Ando, M. (1975), Source mechanisms and tectonic significance of historical earthquakes along the Nankai Trough, *Tectonophysics*, *27*, 119–140.

Beanland, S., A. Melhuish, A. Nicol, and J. Ravens (1998), Structure and deformational history of the inner forearc region, Hikurangi subduction margin, New Zealand, *N. Z. J. Geol. Geophys.*, *41*, 325–342.

Becker, K., A. T. Fisher, and E. E. Davis (1997), The CORK experiment in Hole 949C: Long-term observations of pressure and temperature in the Barbados accretionary prism, *Proc. Ocean Drill. Program Sci. Results*, *156*, 247–252.

Bekins, B. A., and E. J. Screaton (2006), Pore pressure and fluid flow in the northern Barbados accretionary complex: A synthesis, in *The Seismogenic Zone of Subduction Thrust Faults*, edited by T. Dixon and J. C. Moore, Columbia Univ. Press, in press.

Bilek, S. L., and T. Lay (2002), Tsunami earthquakes possibly widespread manifestations of frictional conditional stability, *Geophys. Res. Lett.*, *29*(14), 1673, doi:10.1029/2002GL015215.

Breen, N. A., and D. L. Orange (1992), The effects of fluid escape on accretionary wedges: 1. Variable porosity and wedge convexity, *J. Geophys. Res.*, *97*, 9265–9275.

Brown, K. M., A. Kopf, M. B. Underwood, and J. L. Weinberger (2003), Compositional and fluid pressure controls on the state of stress on the Nankai subduction thrust: A weak plate boundary, *Earth Planet. Sci. Lett.*, *214*, 589–603, doi:10.1016/S0012-821X(03)00388-1.

Byrne, D. E., D. M. Davis, and L. R. Sykes (1988), Local and maximum size of thrust earthquakes and the mechanics of the shallow region of subduction zones, *Tectonics*, *7*, 833–857.

Christensen, D. H., and S. L. Beck (1994), The rupture process and tectonic implications of the great 1964 Prince William Sound earthquake, *Pure Appl. Geophys.*, *142*, 29–53.

Clift, P., and P. Vannucchi (2004), Controls on tectonic accretion versus erosion in subduction zones: Implications for the origin and recycling of the continental crust, *Rev. Geophys.*, *42*, RG2001, doi:10.1029/2003RG000127.

Cummins, P. R., and Y. Kaneda (2000), Possible splay fault slip during the 1946 Nankai earthquake, *Geophys. Res. Lett.*, *27*, 2725–2728.

Currie, C. A., R. D. Hyndman, K. Wang, and V. Kostoglodov (2002), Thermal models of the Mexico subduction zone: Implications for the megathrust seismogenic zone, *J. Geophys. Res.*, *107*(B12), 2370, doi:10.1029/2001JB000886.

Dahlen, F. A. (1984), Noncohesive critical Coulomb wedges: An exact solution, *J. Geophys. Res.*, *89*, 10,125–10,133.

Dahlen, F. A. (1990), Critical taper model of fold-and-thrust belts and accretionary wedges, *Annu. Rev. Earth Planet. Sci.*, *18*, 55–99.

Dahlen, F. A., J. Suppe, and D. Davis (1984), Mechanics of fold-and-thrust belts and accretionary wedges: Cohesive Coulomb theory, *J. Geophys. Res.*, *89*, 10,087–10,101.

Davis, D. M., and R. von Huene (1987), Inferences on sediment strength and fault friction from structures at the Aleutian trench, *Geology*, *15*, 517–522.

Davis, D. M., J. Suppe, and F. A. Dahlen (1983), Mechanics of fold-and-thrust belts and accretionary wedges, *J. Geophys. Res.*, *88*, 1153–1172.

Davis, E. E., K. Becker, K. Wang, K. Obara, and Y. Ito (2006), A discrete episode of seismic and aseismic deformation of the Nankai subduction zone accretionary prism and incoming Philippine Sea plate, *Earth Planet. Sci. Lett.*, *242*, 73–84.

Dewhurst, D. N., M. B. Clennell, K. M. Brown, and G. K. Westbrook (1996), Fabric and hydraulic conductivity of sheared clays, *Géotechnique*, *46*, 761–768.

Enlow, R. L., and P. O. Koons (1998), Critical wedges in three dimensions: Analytical expressions from Mohr-Coulomb constrained perturbation analysis, *J. Geophys. Res.*, *103*, 4897–4914.

Fletcher, R. C. (1989), Approximate analytical solutions for a cohesive fold-and-thrust wedge: Some results for lateral variation in wedge properties and for finite wedge angle, *J. Geophys. Res.*, *94*, 10,347–10,354.

Foucher, J. P., P. Henry, and F. Harmegnies (1997), Long-term observations of pressure and temperature in Hole 948D, Barbados accretionary prism, *Proc. Ocean Drill. Program Sci. Results*, *156*, 239–245.

Freymueller, J. T., C. Zweck, H. Fletcher, S. Hreinsdttir, S. C. Cohen, and M. Wyss (2001), The great Alasak "earthquake" of 1998–2001, *Eos. Eos Trans. AGU*, *82*(47), Fall Meet. Suppl., Abstract G22D-11.

Fruehn, J., R. von Huene, and M. A. Fisher (1999), Accretion in the wake of terrane collision: The Neogene accretionary wedge off Kenai Peninsula, Alaska, *Tectonics*, *18*, 263–277.

Gagnon, K., C. D. Chadwell, and E. Norabuena (2005), Measuring the onset of locking in the Peru–Chile trench with GPS and acoustic measurements, *Nature*, *434*, 205–208.

Gulick, S. P. S., A. M. Meltzer, and S. H. Clarke Jr. (1998), Seismic structure of the southern Cascadia subduction zone and accretionary prism north of the Mendocino triple junction, *J. Geophys. Res.*, *103*, 27,207–27,222.

Gulick, S. P. S., N. L. B. Bangs, T. H. Shipley, Y. Nakamura, G. Moore, and S. Kuramoto (2004), Three-dimensional architecture of the Nankai accretionary prism's imbricate thrust zone off Cape Muroto, Japan: Prism reconstruction via en echelon thrust propagation, *J. Geophys. Res.*, *109*, B02105, doi:10.1029/2003JB002654.

Hayward, N., G. K. Westbrook, and S. Peacock (2003), Seismic velocity, anisotropy, and fluid pressure in the Barbados accretionary wedge from an offset vertical seismic profile with seabed sources, *J. Geophys. Res.*, *108*(B11), 2515, doi:10.1029/2001JB001638.

Henry, P. (2000), Fluid flow at the toe of the Barbados accretionary wedge constrained by thermal, chemical, and hydrogeologic observations and models, *J. Geophys. Res.*, *105*, 25,855–25,872.

Hsu, Y.-J., M. Simons, J.-P. Avouac, J. Galetzka, K. Sieh, M. Chlieh, D. Natawidjaja, L. Prawirodirdjo, and Y. Bock (2006), Frictional afterslip following the 2005 Nias-Simeulue earthquake, Sumatra, *Science*, in press.

Hu, Y., and K. Wang (2006), Bending-like behavior of wedge-shaped thin elastic fault blocks, *J. Geophys. Res.*, *111*, B06409, doi:10.1029/2005JB003987.

Husen, S., E. Kissling, and E. R. Flueh (2000), Local earthquake tomography of shallow subduction in north Chile: A combined onshore and offshore study, *J. Geophys. Res.*, *105*, 28,183–28,198.

Hyndman, R. D., and E. E. Davis (1992), A mechanism for the formation of methane hydrate and seafloor bottom-simulating reflectors by vertical fluid expulsion, *J. Geophys. Res.*, *97*, 7025–7041.

Hyndman, R. D., and K. Wang (1993), Thermal constraints on the zone of major thrust earthquake failure: The Cascadia subduction zone, *J. Geophys. Res.*, *98*, 2039–2060.

Ito, Y., and K. Obara (2006), Dynamic deformation of the accretionary prism excites very low frequency earthquakes, *Geophys. Res. Lett.*, *33*, L02311, doi:10.1029/2005GL025270.

Kopp, H., and N. Kukowski (2003), Backstop geometry and accretionary mechanics of the Sunda margin, *Tectonics*, *22*(6), 1072, doi:10.1029/2002TC001420.

Kukowski, N., T. Schillhorn, K. Huhn, U. von Rad, S. Husen, and E. Flueh (2001), Morphotectonics and mechanics of the central Makran accretionary wedge off Pakistan, *Mar. Geol.*, *173*, 1–19.

Lallemand, S. E., P. Schnürle, and J. Malavieille (1994), Coulomb theory applied to accretionary and nonaccretionary wedges: Possible causes for tectonic erosion and/or frontal accretion, *J. Geophys. Res.*, *99*, 12,033–12,055.

Lohrmann, J., N. Kukowski, J. Adam, and O. Oncken (2003), The impact of analogue material properties on the geometry, kinematics, and dynamics of convergent sand wedges, *J. Struct. Geol.*, *25*, 1691–1711.

Magee, M. E., and M. D. Zoback (1993), Evidence for a weak interplate thrust fault along the northern Japan subduction zone and implications for the mechanics of thrust faulting and fluid expulsion, *Geology*, *21*, 809–812.

Mandal, N., A. Chattopadhyay, and S. Bose (1997), Imbricate thrust spacing: Experimental and theoretical analyses, in *Evolution of Geological Structures in Micro- to Macro-scales*, edited by S. Sengupta, pp. 143–165, CRC Press, Boca Raton, Fla.

Marone, C., and D. M. Saffer (2006), Fault friction and the upper transition from seismic to aseismic faulting, in *The Seismogenic Zone of Subduction Thrust Faults*, edited by T. Dixon and J. C. Moore, Columbia Univ. Press, in press.

Marone, C., C. H. Scholz, and R. Bilham (1991), On the mechanics of earthquake afterslip, *J. Geophys. Res.*, *96*, 8441–8452.

McIntosh, K. D., E. A. Silver, I. Ahmed, A. Berhorst, C. R. Ranero, R. K. Kelly, and E. R. Flueh (2006), The Nicaragua convergent margin: Seismic reflection imaging of the source of a tsunami earthquake, in *The Seismogenic Zone of Subduction Thrust Faults*, edited by T. Dixon and J. C. Moore, Columbia Univ. Press, in press.

McNeill, L. C., K. A. Piper, C. Goldfinger, L. D. Kulm, and R. S. Yeats (1997), Listric normal faulting on the Cascadia continental margin, *J. Geophys. Res.*, *102*, 12,123–12,138.

Moore, D. E., and D. A. Lockner (2006), Friction of the smectite clay montmorillonite: A review and interpretation of data, in *The Seismogenic Zone of Subduction Thrust Faults*, edited by T. Dixon and J. C. Moore, Columbia Univ. Press, in press.

Moore, J. C., and D. Saffer (2001), Updip limit of the seismogenic zone beneath the accretionary prism of southwest Japan: An effect of diagenetic to low grade metamorphic processes and increasing effective stress, *Geology*, *29*, 183–186.

Moore, J. C., and P. Vrolijk (1992), Fluids in accretionary prisms, *Rev. Geophys.*, *30*, 113–135.

Obara, K., and Y. Ito (2005), Very low frequency earthquakes excited by the 2004 off the Kii peninsula earthquakes: A dynamic process in the large accretionary prism, *Earth Planets Space*, *57*, 321–326.

Oleskevich, D. A., R. D. Hyndman, and K. Wang (1999), The updip and downdip limits to great subduction zone earthquakes: Thermal and structural models of Cascadia, south Alaska, SW Japan, and Chile, *J. Geophys. Res.*, *104*, 14,956–14,991.

Ozawa, S., M. Murakami, M. Kaidzu, T. Tada, T. Sagiya, Y. Hatanaka, H. Yarai, and T. Nishimura (2002), Detection and monitoring of ongoing aseismic slip in the Tokai region, central Japan, *Science*, *298*, 1009–1012.

Park, J. O., T. Tsuru, S. Kodaira, P. R. Cummins, and Y. Kaneda (2002), Splay fault branching along the Nankai subduction zone, *Science*, *297*, 1157–1160.

Peacock, S. M., and R. D. Hyndman (1999), Hydrous minerals in the mantle wedge and the maximum depth of subduction zone earthquakes, *Geophys. Res. Lett.*, *26*, 2517–2520.

Plafker, G. (1972), Alaskan earthquake of 1964 and Chilean earthquake of 1960: Implications for arc tectonics, *J. Geophys. Res.*, *77*, 901–925.

Saffer, D. M., and B. A. Bekins (2002), Hydrologic controls on the morphology and mechanics of accretionary wedges, *Geology*, *30*, 271–274.

Sallarès, V., and C. R. Ranero (2005), Structure and tectonics of the erosional convergent margin off Antofagasta, north Chile (23°30′S), *J. Geophys. Res.*, *110*(B6), B06101, doi:10.1029/2004JB003418.

Scholz, C. H. (2003), *The Mechanics of Earthquakes and Faulting*, 2nd ed., 471 pp., Cambridge Univ. Press, New York.

Schott, B., and H. A. Koyi (2001), Estimating basal friction in accretionary wedges from the geometry and spacing of frontal faults, *Earth Planet. Sci. Lett.*, *194*, 221–227.

Sibson, R. H. (1981), Fluid flow accompanying faulting: Field evidence and models, in *Earthquake Prediction: An International Review*, *Maurice Ewing Ser.*, vol. 4, edited by D. W. Simpson and P. G. Richards, pp. 593–603, AGU, Washington, D. C.

Uchida, N., T. Matsuzawa, and A. Hasegawa (2003), Interplate quasi-static slip off Sanriku, NE Japan, estimated from repeating earthquakes, *Geophys. Res. Lett.*, *30*(15), 1801, doi:10.1029/2003GL017452.

von Huene, R., and D. Klaeschen (1999), Opposing gradients of permanent strain in the aseismic zone and elastic strain across the seismogenic zone of the Kodiak shelf and slope, Alaska, *Tectonics*, *18*, 248–262.

von Huene, R., and S. Lallemand (1990), Tectonic erosion along the Japan and Peru convergent margin, *Geol. Soc. Am. Bull.*, *102*, 704–720.

von Huene, R., and C. R. Ranero (2003), Subduction erosion and basal friction along the sediment-starved convergent margin off Antofagasta, Chile, *J. Geophys. Res.*, *108*(B2), 2079, doi:10.1029/2001JB001569.

von Huene, R., and D. W. Scholl (1991), Observations at convergent margins concerning sediment subduction, erosion, and the growth of continental crust, *Rev. Geophys.*, *29*, 279–316.

von Huene, R., C. R. Ranero, and P. Vannucchi (2004), Generic model of subduction erosion, *Geology*, *32*(10), 913–916.

Wang, K. (2004), Understanding processes and estimating parameters using mathematical models, in *Hydrogeology of the Oceanic Lithosphere*, edited by E. Davis and H. Elderfield, pp. 376–413, Cambridge Univ. Press, New York.

Wang, K., and T. Dixon (2004), "Coupling" semantics and science in earthquake research (Forum article), *Eos Trans. AGU*, *85*, 180.

Wang, K., and J. He (1999), Mechanics of low-stress forearcs: Nankai and Cascadia, *J. Geophys. Res.*, *104*, 15,191–15,205.

Wang, K., T. Mulder, G. Rogers, and R. Hyndman (1995), Case for very low coupling stress on the Cascadia subduction fault, *J. Geophys. Res.*, *100*, 12,907–12,918.

Wang, W. H., and D. M. Davis (1996), Sandbox model simulation of forearc evolution and noncritical wedges, *J. Geophys. Res.*, *101*, 11,329–11,339.

Wells, R. E., R. J. Blakely, Y. Sugiyama, D. W. Scholl, and P. A. Dinterman (2003), Basin-centered asperities in great subduction zone earthquakes: A link between slip, subsidence, and subduction erosion?, *J. Geophys. Res.*, *108*(B10), 2507, doi:10.1029/2002JB002072.

Willett, S., C. Beaumont, and P. Fullsack (1993), Mechanical model for the tectonics of doubly vergent compressional orogens, *Geology*, *21*, 371–374.

Xiao, H. B., F. A. Dahlen, and J. Suppe (1991), Mechanics of extensional wedges, *J. Geophys. Res.*, *96*, 10,301–10,318.

Zhao, W. L., D. M. Davis, F. A. Dahlen, and J. Suppe (1986), Origin of convex accretionary wedges: Evidence from Barbados, *J. Geophys. Res.*, *91*, 10,246–10,258.

Y. Hu, School of Earth and Ocean Sciences, University of Victoria, Victoria, BC, Canada V8P 5C2. (yanhu@uvic.ca)

K. Wang, Pacific Geoscience Centre, Geological Survey of Canada, 9860 West Saanich Road, Sidney, BC, Canada V8L 4B2. (kwang@nrcan.gc.ca)